ELSEVIER

Marine Geology 211 (2004) 79–99

MARINE GEOLOGY
INTERNATIONAL JOURNAL OF MARINE GEOLOGY, GEOCHEMISTRY AND GEOPHYSICS

www.elsevier.com/locate/margeo

Sedimentary facies and high resolution primary production inferences from laminated diatomacous sediments off northern Chile (23°S)

Gabriel Vargas[a,b,*], Luc Ortlieb[b], Jean Jacques Pichon[a,†], Jacques Bertaux[b,†], Michel Pujos[a]

[a]*UMR-CNRS 5805 EPOC, Université Bordeaux I, Avenue des Facultés, 33405 Talence Cédex, France*
[b]*UR55-Paléotropique, Institut de Recherche pour le Développement, 32 Avenue Henri Varagnat, 93143 Bondy Cédex, France*

Received 13 August 2002; received in revised form 28 May 2004; accepted 28 May 2004

Abstract

The oceanographic conditions at the Mejillones bay (23°S) are strongly influenced by an important wind-driven upwelling cell of the Humboldt Current System (HCS), as well as by the presence of the Oxygen Minimum Zone (OMZ) in this region. Laminated diatomaceous sediments in this bay were analysed using different qualitative and quantitative techniques on the sediment cores 33C and 32B, to interpret the main physical ocean–climate factors driving sedimentation processes. The composition of these sediments is dominated by the high concentration of resting spores of the genus *Chaetoceros* sp., which denotes the strong influence of the upwelling events and primary production on hemipelagic sedimentation processes within the basin. The laminae, characterized by thickness ranging from 1 mm to several cm, are associated with changes in density (/porosity) due to the different concentration and composition of phytoplankton remains and organic matter. Dark laminae are generally characterized by higher concentration of *Chaetoceros r.s.*, TOC, organic matter, carbonates and lithic minerals with respect to the adjacent lighter laminae, representing periods of strong upwelling events, high primary production rates and intensified hypoxia. Contrarily, relatively lighter laminae are characterized by diminished concentration of *Chaetoceros r.s.* and relative increases of the concentration of centric and pennate diatoms, producing a more porous sediment. Some of these light laminae could be associated with short-lived major oceanographic ENSO-like events.

The variability of the sedimentary fluxes observed in both cores represents mostly ocean–climate trends at decadal, interdecadal and secular time periods. The secular trends of the sedimentary fluxes suggest an intensification of the upwelling events and primary production from the second half of the 19th century, as well as intensified processes during the 20th century.

* Corresponding author. Present address: Departamento de Geología, Facultad de Ciencias Físicas y Matemáticas, Universidad de Chile, Plaza Ercilla 803, Santiago, Chile.
E-mail address: gvargas@ing.uchile.cl (G. Vargas).
† Deceased.

doi:10.1016/j.margeo.2004.05.032

These changes seem to occur contemporaneously with ocean–climate variations in the southwestern tropical Pacific Ocean, suggesting a major basin scale climate change during this period.

Keywords: laminated sediments; diatom ooze; Humboldt Current System; upwelling; primary production; Oxygen Minimum Zone; paleoceanography

1. Introduction

Laminated marine sediments constitute an infrequent and exceptional geological record because of its relevancy for high-resolution paleoceanographic reconstructions. On continental margins, this type of sediment occurs in zones characterized by high primary production rates, normally associated with seasonal, interannual or decadal, ecological or hydrological variations (e.g., Hughen et al., 1996; Bull and Kemp, 1996; Grimm et al., 1997; Staubwasser and Sirocko, 2001). In areas where Oxygen Minimum Zones (OMZs) intercept the shelf, inducing bottom hypoxia, bioturbation processes are limited and the preservation of laminae is favoured. The understanding of the origin of this type of sedimentary record, which is a necessary stage before interpreting ocean–climate variability, normally involves a multidisciplinary approach, including high resolution qualitative and quantitative sedimentological, geochemical, micropaleontological and geochronological analyses.

Among natural earth systems, upwelling areas constitute one of the most compelling examples of air–sea interactions with ecological impacts. These areas play a major role in ocean–atmosphere exchanges of CO_2 and other greenhouse gases. This is particularly true in highly productive eastern boundary currents as the Humboldt Current System (HCS), where recent data suggest important CO_2 outgassing during strong upwelling events (Torres et al., 1999, 2002), as the result of complex exchanges in the OMZ (Morales et al., 1996). Given that the tropical Pacific Ocean is considered the greatest natural source of CO_2 to the atmosphere (>1 Gt C year^{-1}; Takahasi, 1989), the study of high resolution geological records from this area is specially relevant.

Works focusing on natural evolution of the HCS at subtropical and midlatitudes during the Late Quaternary, suggest important ocean–climate variations through the last glacial–interglacial period (Marchant et al., 1999; Lamy et al., 1999, 2000; Kim et al., 2002; Hebbeln et al., 2002). Laminated marine sediments have been reported off northern Chile near an important upwelling centre (Mejillones bay, 23°S), suggesting great potential for paleoceanographic reconstructions at high time frequencies (Ortlieb et al., 2000; Valdés et al., 2003). In this paper, we analyse the composition and structure of these sediments, to interpret the main physical ocean–climate mechanisms controlling their formation, as well as the most evident patterns of ocean–climate variations during the last few centuries.

1.1. Ocean–climate setting and upwelling dynamic

According to Strub et al. (1998), the regional circulation off northern Chile is dominated by the Humboldt (Peru–Chile) Current, transporting Subantartic Water (11.5 °C<T<14.5 °C, 34.1<S<34.8) from higher to lower latitudes (Fig. 1). The Peru–Chile Countercurrent (PCCC), which is associated with Subtropical Surface Water (T>18.5 °C, S>34.9), divides it into an oceanic and a coastal branch. The Poleward Undercurrent (PUC) underlies the Humboldt Current and PCCC, transporting Equatorial Subsurface Water (ESSW) (8.5 °C<T<10.5 °C, 34.4<S<34.8) to the south. ESSW is characterized by low concentrations of oxygen ([O_2]<0.25–0.5 ml l^{-1}), defining the OMZ off northern Chile between 50 and 300 m of water depth (Brandhorst, 1971; Morales et al., 1996). Below 500 m, Antarctic Intermediate Water (T~5.5 °C, 34.3<S<34.5) flows toward the equator.

Along the coast off northern Chile, the Pacific Subtropical Anticyclone (PSA) drives upwelling-favourable equatorward winds during the entire year, reinforced during spring and summer by strong air–land–sea interactions (Schwerdtfeger, 1976; Lettau and Lettau, 1978; Strub et al., 1998) (Fig. 1).

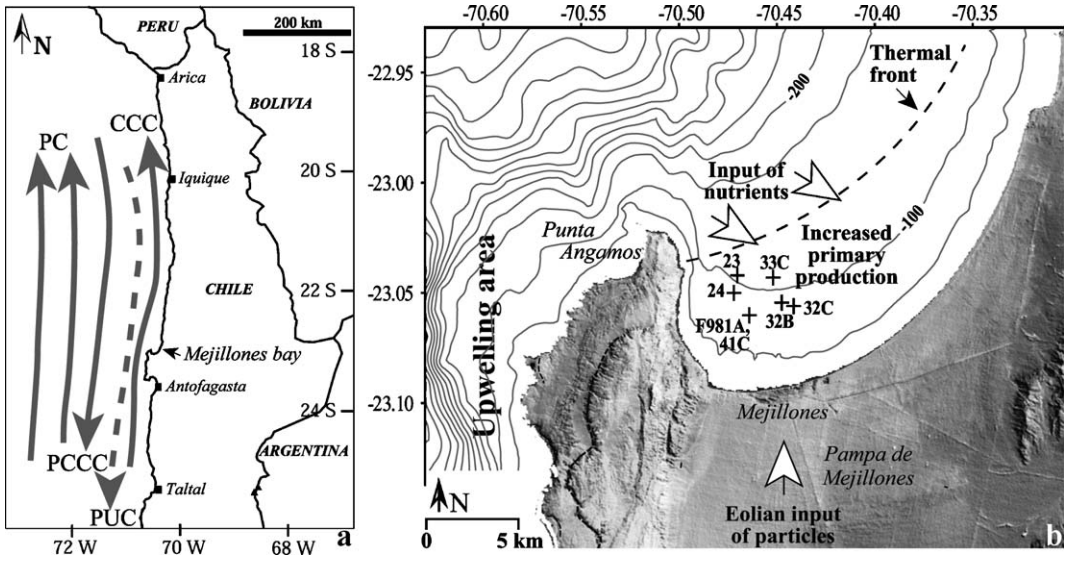

Fig. 1. (a) Major components of the Humboldt Current System during the spring and summer off northern Chile, according to Strub et al. (1998). PC: Peru Current; PCCC: Peru–Chile Counter Current; PUC: Poleward Undercurrent; CCC: Chile Coastal Current. (b) Bathymetry and oceanographic context of the Mejillones bay, indicating the main elements to explain the increased primary production within the bay (Marín and Olivares, 1999; Marín et al., 2003). The input of aeolian particles due to the dominant S–SW winds is also indicated. Cores 33C and 32B were retrieved from the central part of the bay, at around 100 m of water depth. The location of other cores used for a lateral correlation and chronological determination (Vargas et al., in press) is also shown.

Upwelling events are driven by relaxation-reinforcing cycles (4–15 days) in the strength of SW winds associated to the poleward propagation of atmospheric coastal lows (Rodríguez et al., 1991; Marín et al., 1993; Rutllant et al., 1998). The upwelling system at Punta Angamos (Navea and Miranda, 1980; Rodríguez et al., 1991) drives high primary production rates within the Mejillones bay (1070 g C m^{-2} $year^{-1}$ estimated for the period 1990–1991; Marín et al., 1993). In situ data show that the composition of phytoplankton is largely dominated by diatoms (between 47% and 100% of the total cells), with *Chaetoceros* sp. as the dominant genus, dinoflagellates (between 0 and 50%) and low concentrations of silicoflagellates, with higher numbers of total cells and species during the spring and summer, with respect to winter and autumn (Rodríguez and Escribano, 1996).

Using in situ measurements and remote sensing data, Marín and Olivares (1999) proposed that the high primary production rates observed in the inner part of the bay are ultimately forced by two climate factors: the intensification of the SW wind and the solar radiation. Marín et al. (2003) proposed that the Mejillones Bay acts as an upwelling shadow subsystem (Graham and Largier, 1997), isolated from the rest of the Mejillones ecosystem by a thermal front. This subsystem results from the interaction between the regional flow and the coastal Ekman dynamics associated with the upwelling of cold waters, during the intensification of the SW winds (Marín et al., 2001; Fig. 1). Primary production rates, estimated as 4–8 t C km^{-2} day^{-1} within the bay, are favoured by a restricted oceanic circulation and low turbulence, the input of nutrients to the photic zone and the solar radiation, which also induces the stabilization of a well stratified water column because of the heating of the surface layer (Marín and Olivares, 1999; Marín et al., 2003; Fig. 2). Low oxygen concentrations ($[O_2]<1$ ml l^{-1}), partly associated with the OMZ, characterize most of the water column at depths below 50 m, while hypoxic and near anoxic conditions ($[O_2]<0.1$ ml l^{-1} at depths greater than 50 m) are normally found at the sea bottom (Escribano, 1998; Fig. 2). These conditions are sporadically broken during the poleward propagation of Kelvin waves associated with El Niño events, causing SST warming and deepening of the thermocline and oxycline, which seems to induce diminished primary production rates offshore the

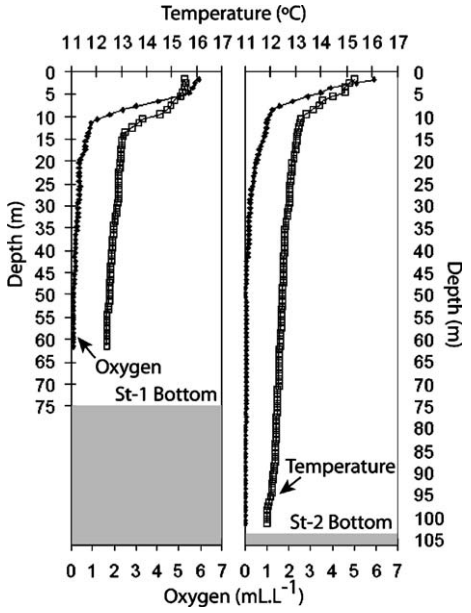

Fig. 2. Temperature and oxygen profiles taken at stations 1 and 2 in October 1998, which are close to the location of cores F981A (Fig. 1) and 33C, respectively. Both profiles show the strong stratification of the water column, with a well-developed and shallow thermocline and oxycline within the bay.

Mejillones peninsula (Gonzalez et al., 1998, 2000; Iriarte et al., 2000; Ulloa et al., 2001).

1.2. The sedimentary record at Mejillones bay

Mejillones bay is a small and shallow marine sedimentary basin (15 km diameter, 125 m of maximum depth), protected from the direct influence of the SW winds by the Mejillones peninsula (Fig. 1). From paleoecological interpretations based on foraminifera rests, fish scales and diatom skeletons counted along sedimentary cores, Ortlieb et al. (2000) attempted to reconstruct significant secular ocean–climate variations during the last millennia. Based on similar Fourier transform infrared (FTIR) spectra of soluble organic matter from these sediments and those from phytoplankton sources, Valdés et al. (2000) suggested high preservation and negligible effect of early diagenesis on the sedimentary organic fraction. Taking into account the restricted alluvial input due to the extreme aridity that characterizes the coastal Atacama Desert in this region (Vargas et al., 2000), the bay acts as a natural trap for pelagic sedimentation induced by the upwelling processes at Punta Angamos. Some new results from downcore ^{14}C and ^{210}Pb data suggest mass accumulation rates about 0.034–0.027 g cm^{-2} $year^{-1}$ (0.170–0.130 cm $year^{-1}$) at the centre of the basin (Vargas et al., in press), confirming the great potential of this record for ocean–climate reconstructions from pluri-annual to secular time periods.

2. Materials and methods

2.1. Coring and X-ray analyses

The cores 33C and 32B (66 and 44 cm long, respectively) were collected in 1996 using a 3-in.-diameter gravity corer and were then preserved at 4 °C (Fig. 1). X-ray images were taken using conventional medical equipment, with mean exposure parameters of about 50 kV, during 0.16 s and 1 m of distance. Contact prints (positive phases) were then produced and treated with specialised softwares to obtain the grey-level intensity scale (GL). The GL (ranging from 0-light to 255-dark in positive phases), which reflects the penetration of the X-rays through the analysed material, depends upon the density, the atomic number and the thickness of the sample (Calvert and Veevers, 1962; Bouma, 1964). Because the sediment thickness is maintained along the entire core, the variability of the GL can be interpreted as a function of the variability of the sedimentary density (or porosity) and the nature of the sediment. To provide a comparable dataset between the GL and the other sedimentological properties, the GLMean was calculated as the mean value of the corresponding interval of sampling in each core.

2.2. Chronological models for the cores 33C and 32B

Chronological determinations from detailed ^{14}C and ^{210}Pb downcore data, which involve new hypotheses regarding the relationship between the radiocarbon Local Reservoir Effect (ΔR) and the intensity of the upwelling events, was the matter of a PhD Thesis (Vargas, 2002) and will be published elsewhere. The methodology used to determine mass accumulation rates and chronological models for both cores (33C and 32B) is described in Vargas et al. (in

press). Mass accumulation rates were calculated from (1) calibration of AMS radiocarbon data from 1 cm mean thick samples, using Calib.4.3 for marine datasets (Stuiver and Reimer, 1993) and considering a ΔR=262±13 years, (2) a precise lateral correlation between the cores F981A, 41C, 32B and 33C (Fig. 1), and (3) taking into account the presence of two sedimentological discontinuities located at 45.5 and 47.5 cm depth in the core 33C, and at 43.4 cm depth in the core 32B. The generation of these features has been associated to the effect of local reactivations of faults in the Mejillones peninsula, during two strong earthquakes which occurred between the years 1409–1449 and 1754–1789 AD (Vargas et al., in press). Mass accumulation rates about 0.027 g cm^{-2} year^{-1} (0.156 cm year^{-1}) characterize the entire core 32B and the top 44.5 cm of the core 33C, suggesting that those sequences represent roughly the last 250 years (Fig. 3). Similarly, a mass accumulation rate about 0.011 g cm^{-2} year^{-1} (0.065 cm year^{-1}), calculated from calibrated radiocarbon data, suggests that the bottom segment of the core 33C (48.5–65.5 cm depth) represents the period involving the 11th, 12th and the 13th centuries. The implication of this chronological model is a hiatus of about 250 years in the latter core (Vargas et al., in press).

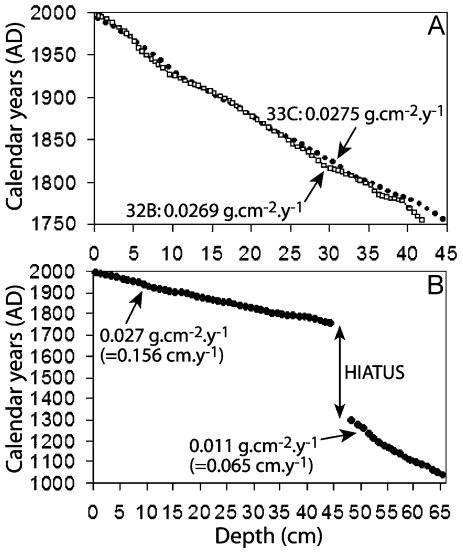

Fig. 3. (A) Mass accumulation rates and chronological models inferred for the top segment of the core 33C and the entire core 32B. (B) Chronological model for the entire core 33C, which involves a hiatus associated with two discontinuities probably generated during strong seismic events occurred at 1409–1449 and 1754–1789 AD (Vargas et al., in press).

2.3. Qualitative and semi-quantitative estimations from thin sections

Thin sections were constructed every 10 cm from resin-impregnated samples of the core 33C, after fractionated replacement of the water by acetone. The structure of the laminations was analysed using a polarised light microscope, with a magnification of ×20. The determination and estimation every mm of the concentration of biogenic remains and lithic minerals were performed using a magnification of ×80. Drawing was made for thin section 2 (10.5–20.5 cm) to show the lamination style and the associated high resolution variability of the components. The identification and estimation of phytoplankton rests within the individual laminae were carried out using a magnification of ×320.

2.4. Quantitative analyses and statistics

Samples for quantification of sedimentological parameters, biogenic rests and lithic minerals were taken every cm in the case of the core 33C, and with a variable thickness in the case of the core 32B, between 0.4 and 1 cm, to respect the limits of the laminations previously observed in the X-ray image.

For the core 33C, the water content (expressed as weight percentage) and the bulk dry density were measured on 1/4 of each sample, drying the sediment at 40–50 °C. Samples were washed and sieved at 500, 160 and 63 μm for the observation of fish scales and foraminifera rests. Fish scales were identified from the coarser fraction by comparison with a reference collection of modern material from the most common fishes in this region. Qualitative and semi-quantitative observations of the foraminifera rests were performed following the method described by Páez et al. (2001). Among these rests, the occurrence of *Bolivina seminuda*, which has been described as the dominant benthic species in superficial sediments associated with microxic environments ([O_2]<0.01 ml l^{-1}) in this bay, can be taken as an evidence of dominant hypoxic conditions within the basin.

Diatom slides were prepared for every 1 cm interval samples from the core 33C, using the settling technique

fully described by Rathburn et al. (1997) and fixed in Naphrax (n_c=1.65). Diatom counts follow the Schrader and Gersonde (1978) and Laws (1983) technique. Phytoplankton species were identified and a minimum of 300 diatom valves were counted into each sample using a Zeiss photomicroscope at a magnification of ×1000, and then expressed in millions of valves per gram. Relative quantities of phytoplankton families or species are expressed as the percentage from the total phytoplankton valves, while absolute quantities are expressed in millions of valves per gram.

FTIR analysis was performed in transmission mode to quantify the relative variations in the concentration of lithic minerals, carbonates and amorphous silica (opal) in both cores, following the method described in Bertaux et al. (1998). The FTIR spectra (mid-infrared frequency range: 2.5–40 μm) were measured on 300 mg of a preparation of bulk sediment mixed with KBr, and then compared with reference mineralogical spectra. Quantities are expressed as wt.% of the total dry sediment. A precision of ±1% is estimated for each individual determination (Bertaux et al., 1998).

The Total Organic Carbon (TOC, expressed as wt.%), with an analytical error <0.3%, and the Hydrogen Index (HI), expressed as mg HC/g C_{org}, were determined in both cores using the Rock–Eval pyrolysis (Espitalié et al., 1977). The content of nitrogen (N, expressed as wt.%) in sediment samples was measured using a *Fisons*-CHN-analyser after decalcification in $HCl_{10\%}$, given an analytical error <0.02%. C/N values were calculated as the ratio between TOC and N.

Sedimentary fluxes were calculated considering the mass accumulation rates characteristic of the top segment of the core 33C and the core 32B. In the case of those components expressed in wt.%, the corresponding sedimentary flux was calculated as: $F_{Ax}=10\times[A]_x\times W_{core}$, where $[A]_x$ is the concentration of the component A, expressed in wt.%, at the level x, W_{core} is the mass accumulation rate corresponding to the respective core and F_{Ax} is the calculated flux of the component A at the level x, expressed in mg cm^{-2} $year^{-1}$. Fluxes of phytoplankton rests were calculated as: $F_{Px}=P_x\times W_{core}$, where P_x is the concentration of the corresponding phytoplankton family or species at the level x, expressed as absolute quantities, and F_{Px} is the calculated flux at the level x, expressed in 10^6 valves cm^{-2} $year^{-1}$.

Finally, correlation, linear regression modelling and principal component analyses were carried out to provide statistical support for the different hypotheses realized from the qualitative and quantitative observations.

3. Results

3.1. Microfacies and composition

The general structure of the sedimentary sequences 33C and 32B can be observed in the corresponding X-ray images (Figs. 4 and 5, respectively). In both cores, the successions are composed by well-preserved light and dark laminae ranging in thickness from 1 mm to several cm. The absence of any evidence of bioturbation or hydrodynamic reworking was confirmed through microscopic observations, which also revealed clear limits of laminae (Plate IA). Generally, those limits are abrupt but not marked by physical discontinuities, suggesting that the laminations are associated with a dominant continuous and relatively rhythmic hemipelagic sedimentation process.

X-ray diffraction analyses and FTIR results showed the mineralogical composition of the sediment. Opal (amorphous silica) is the most important component (concentration ranging from 36% to 65% in both cores), reflecting the high content in siliceous phytoplankton skeletons, which was clearly observed in microfacies (Plate I). Among the diatom rests, unfragmented resting spores of *Chaetoceros* sp. (*Chaetoceros r.s.*) is the most abundant genus, confirming the relevancy of the upwelling events driving sedimentation processes within the bay (Plate IA–C). Quantitative analyses, every 1 cm, from samples of the core 33C support this last observation: among the total valves of phytoplankton (Fig. 4), *Chaetoceros r.s.* constitutes between 52% and 89%, centric diatoms represent between 6% and 38%, the concentration of pennate diatoms varies between 1% and 23%, while the occurrence of silicoflagellates is less than 2%. Altogether, the occurrence of agglomerates of different phytoplankton rests as vegetative cells and setae of centric and pennate diatoms correspond most probably to the preservation of faecal pellets (Plate IE). The sporadic occurrence of monospecific levels constituted by large diatom rests

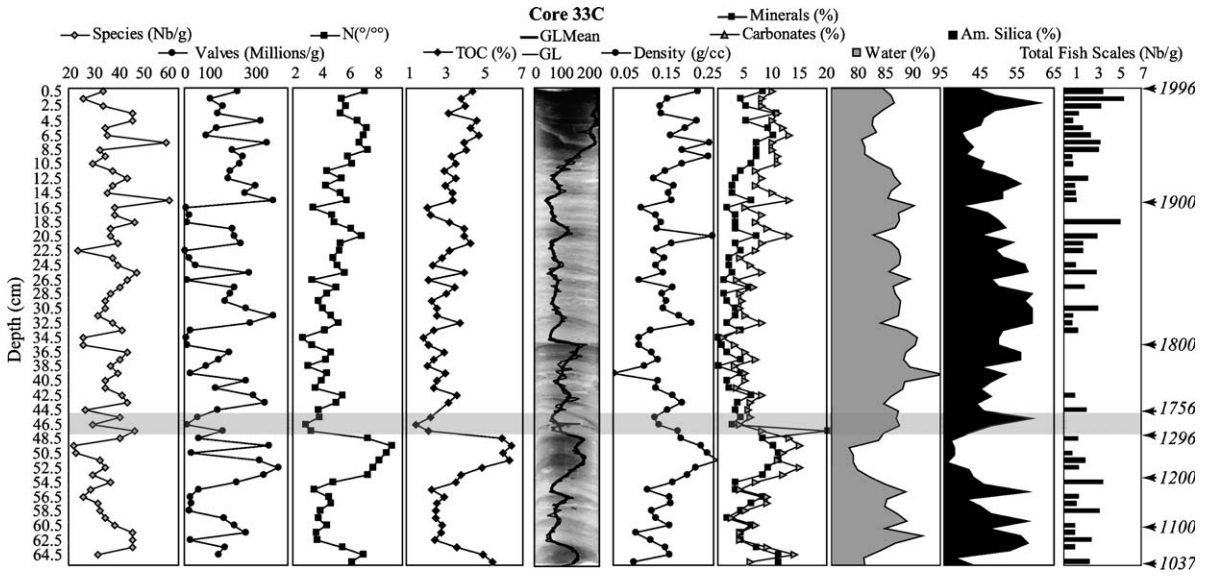

Fig. 4. Quantification, every 1 cm, of the sedimentary components of the core 33C. Species and valves correspond to the total number of species and to the total number of phytoplankton valves per gram of dry sediment within each level. The greyish horizontal bar shows the stratigraphic location of two discontinuities associated with a 450-year hiatus in this core. Calendars years are indicated on the right side.

as *Coscinodiscus gigas* (Plate IF), constitutes an additional evidence for the high degree of preservation of individual laminae.

The high concentration of TOC, ranging from 1.5% to 6.4% and from 2.5% to 6.1% (mean values around 3.4% and 4.6%) in both cores, 33C and 32B, respectively, reflects the organic rich character of these sediments, and supports the interpretation that primary production processes drive high sedimentary fluxes within the basin. The C:N Redfield ratio values of the sedimentary organic matter, around 6.8 and 6.6 in cores 33C and 32B (Figs. 6 and 7), respectively, are close to those characterizing the original phytoplankton-derived organic matter (Meyers, 1994, 1997), suggesting a well-preserved signal from the ocean surface. This last hypothesis is also supported by the total range of variability of the HI, ranging from 389 to 647 mg HC/g C_{org}, which, according to Tissot and Welte (1984) and Meyers (1997), is typical of marine organic matter rich in algae-derived hydrocarbon.

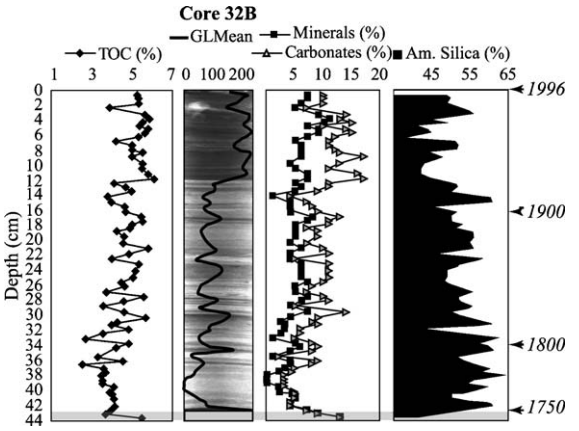

Fig. 5. Quantification of the sedimentary components of the core 32B, considering a variable sampling interval between 0.4 and 1 cm. Calendars years are indicated on the right side.

The carbonate content ranges between 1% and 17%, with mean values near 10% in both cores (Figs. 4 and 5), and can be associated with the occurrence of foraminifera and calcareous phytoplankton rests (Plate IB). Among the rest of foraminifers, the most abundant is the benthic species *B. seminuda*, suggesting persistent hypoxic to microxic conditions during the depositional periods of these sequences (Páez et al., 2001). Taking into account some oceanic surveys developed at 30°S (Marchant et al., 1998), the dominancy of *Globigerina bulloides*, among the planktonic species, seems to confirm that upwelling events induce sedimentation processes within the basin. Altogether, the occurrence of coccoliths, among

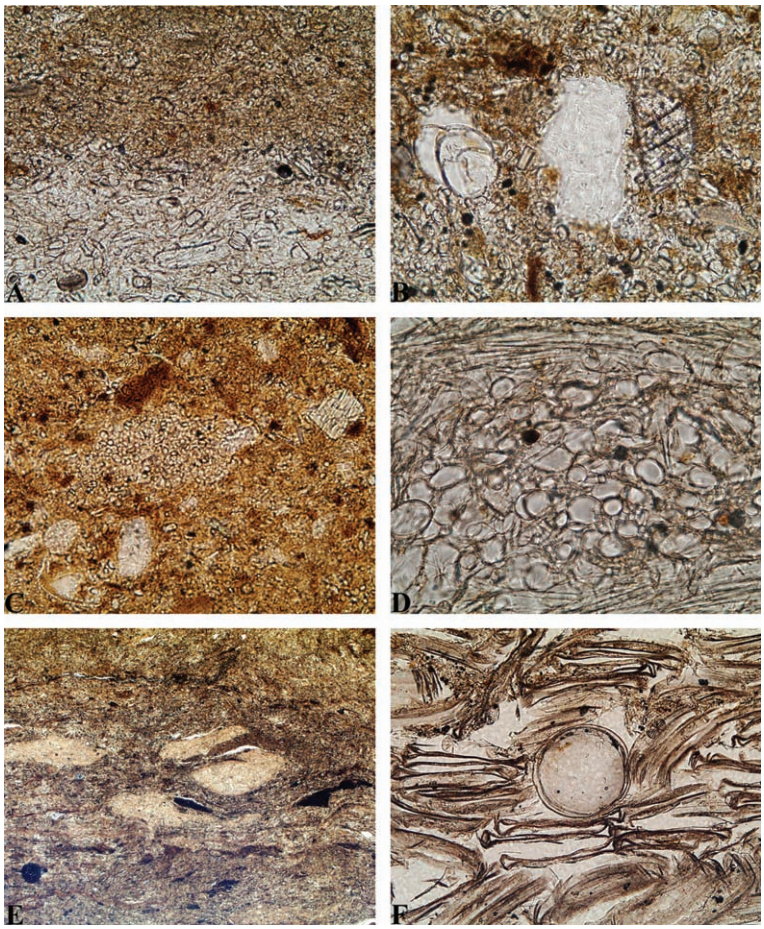

Plate I. (A) Photo: ×200. Contact between a light lamina and the overlying dark lamina, showing the higher concentration of *Chaetoceros r.s.* and organic matter in the dark layer with respect to the more porous light lamina, characterized by relative higher increases of centric diatoms. The contact is abrupt, but not marked by a physical discontinuity. (B) Photo: ×200. Foraminifer remains (*Neogloboquadrina pachyderma*) and lithic grains (quartz and amphibole) within a matrix of *Chaetoceros r.s.* and organic matter, corresponding to a dark lamina. (C) Photo: ×200. Agglomerate of *Chaetoceros r.s.* within a dark layer enriched in organic matter (and agglomerated organic matter (brown), biogenic remains and lithic minerals as quartz and feldspars. (D) Photo: ×400. Agglomerate of *Chaetoceros r.s*. and other phytoplankton remains within a light lamina enriched in pennate diatoms. (E) Photo: ×20. Faecal pellets formed by vegetative cells and setae of diatoms, preserved within dark laminae. (F) Photo: ×100. Monospecific lamina of unfragmented remains of *C. gigas*.

the calcareous phytoplankton rests, was confirmed through microscopic observations of thin sections.

The content in lithic minerals ranges from 0 to 24% (mean value 5%) in both cores (Figs. 4 and 5). The most abundant mineralogical species are quartz and feldspar (albite, oligoclase, microcline; Plate IB), which are abundant in rocks and Quaternary sediments of the Mejillones peninsula (Ferraris and Di Biase, 1978). Amphiboles, chlorite and clay minerals occur in percentages less than 1%. The mean grain size of all these particles, ranging from about 40 to 110 μm (Plate IC; Fig. 8a), as well as the generally chaotic distribution within each individual laminae, support the hypothesis of an aeolian supply of this material from the Mejillones peninsula by the dominant S–SW winds.

3.2. Lamination style and variability of sedimentary components

The general agreement between the variability of all the components and the GLMean, which charac-

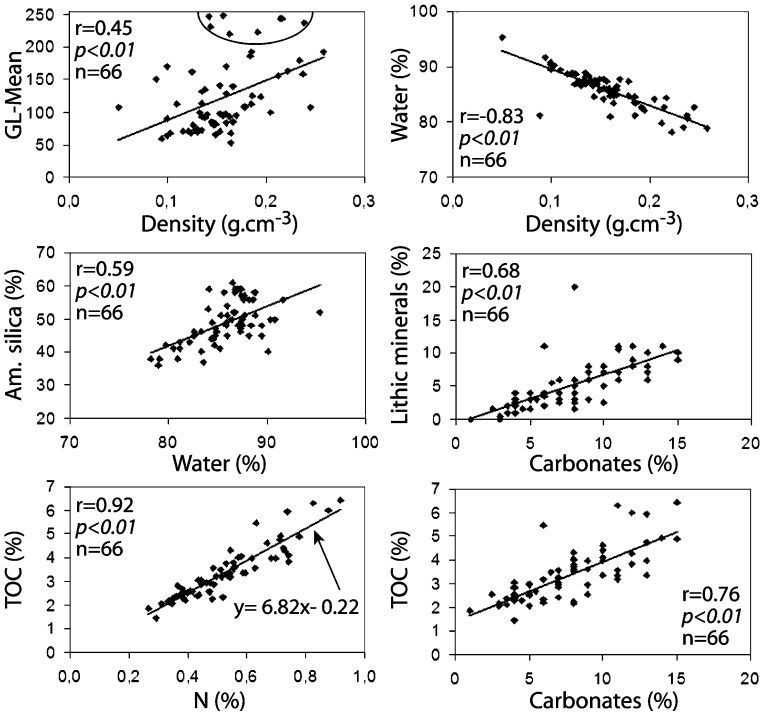

Fig. 6. Correlation between sedimentary parameters and components in the core 33C, indicating the correlation coefficient (r), the robustness of the correlation (p) and the number of cases (n). The weak, but significant, correlation between the GLMean and the sedimentary density can be attributed to some deficiency in the top segment of the X-ray image of this core (Fig. 4), indicated in upper case.

terizes the mean trend of the lamination style, can be observed in Figs. 4 and 5. This suggests that the laminations are associated with physical and compositional changes within the sequences. This hypothesis is supported by the statistical comparison between the variability of the GLMean and other sedimentary

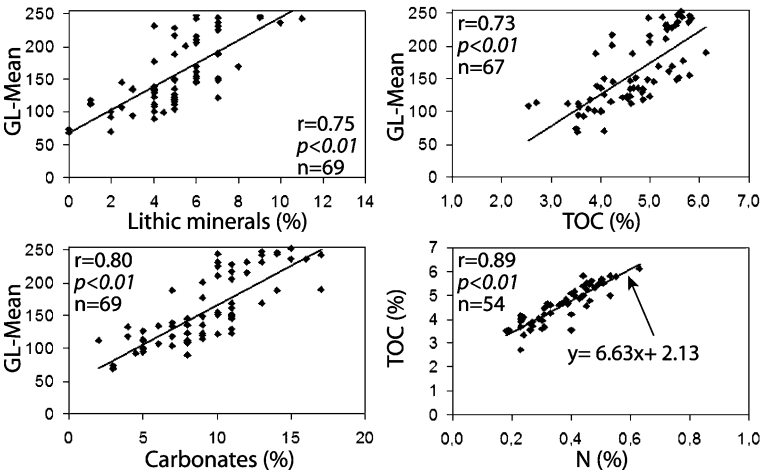

Fig. 7. Correlation between GLMean and sedimentary components in the core 32B, indicating the correlation coefficient (r), the robustness of the correlation (p) and the number of cases (n).

properties (Figs. 6 and 7). The GLMean is significantly correlated with the density and inversely correlated with the water content, suggesting that the dark laminae are generally denser than the light facies (Fig. 6). Observations of microfacies confirm this hypothesis: the dark laminae are enriched in *Chaeto-*

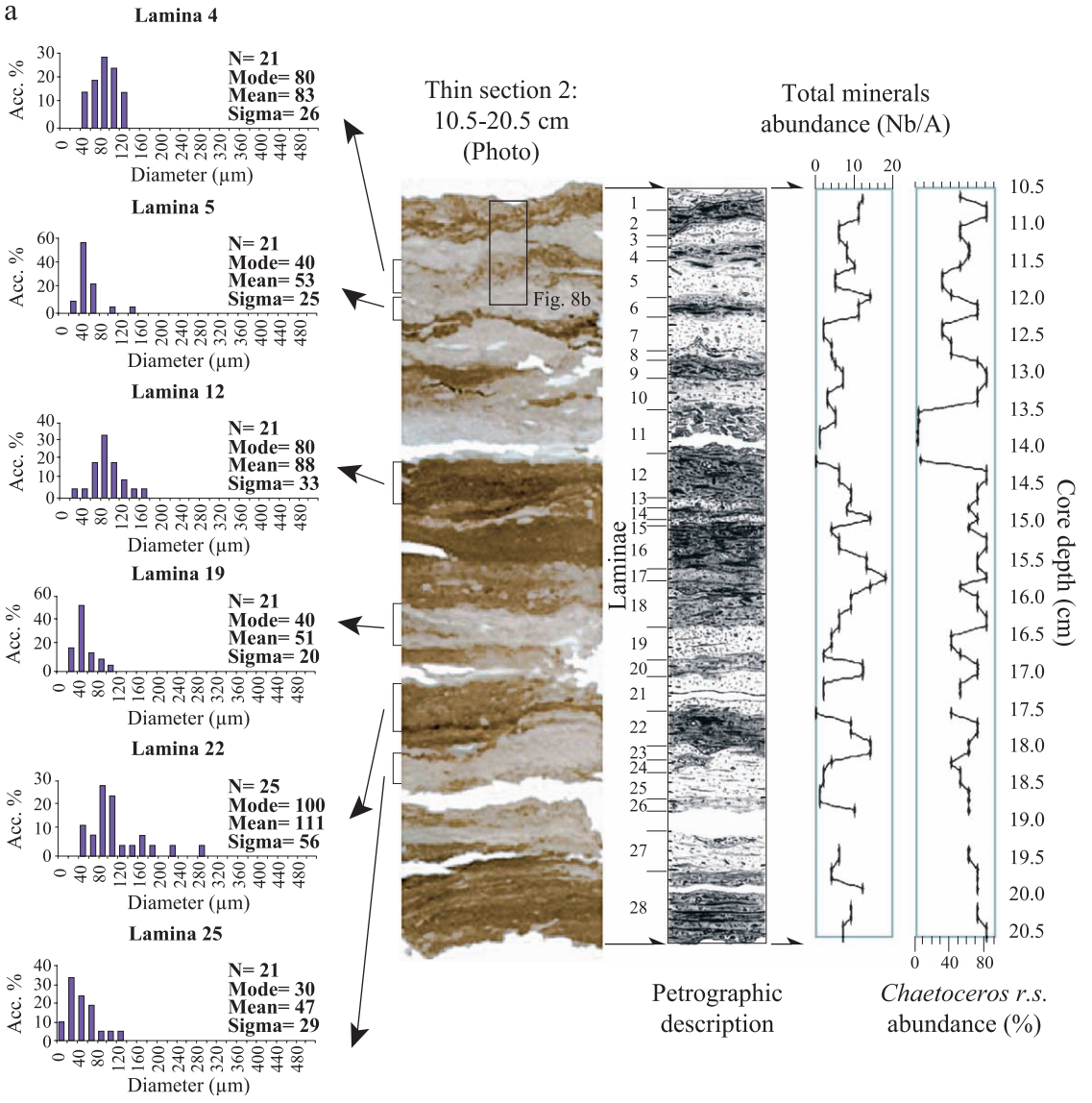

Fig. 8. (a) Photography and petrographic description of the thin section 2 (10.5–20.5 cm core depth), indicating the concentration, every mm, of total minerals (per A=7 mm^2 of section), the concentration, every mm, of *Chaetoceros r.s.* (%) and the grain size distribution of the lithic particles within some of the laminae. (b) A: Detailed view of the first five laminae of the thin section 2, showing different degrees of coloration. The higher concentration of the agglomerated organic matter (brown), lithic minerals and foraminifera rests within the dark laminae with respect to the overlying and underlying lighter laminae can be observed. B: Magnification of the contact between a dark lamina and the overlying light lamina, showing a higher density of *Chaetoceros r.s.* (black arrows) and organic matter within the underlying dark lamina (lamina 4), with respect to the overlying light lamina characterized by higher porosity.

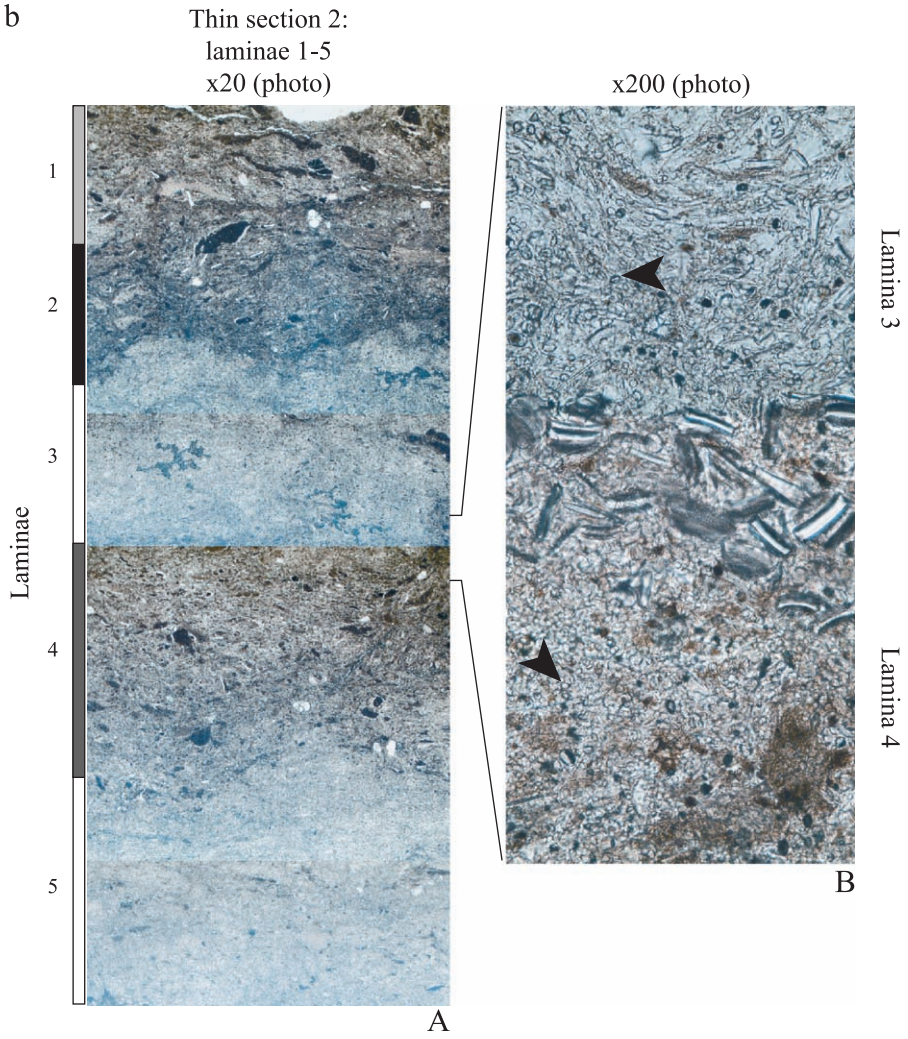

Fig. 8 (*continued*).

ceros r.s., agglomerated organic matter, foraminifera rests and lithic particles, with respect to the adjacent lighter laminae (Figs. 8 and 9). Also, Fig. 8a shows that the mean grain size of the lithic particles within the dark laminae is greater than within the light facies. Contrarily, the lighter laminae are characterized by diminished concentration of *Chaetoceros r.s.* and higher concentration of other pennate and centric diatoms, thus producing a more porous sediment. The statistical support for these observations is given by the significant normal correlation between the GLMean and the concentration of sedimentary components as lithic minerals, carbonates and TOC also (Fig. 7). Moreover, Fig. 6 shows that the concentration in opal is significantly correlated with the water content, because of the relative general diminution of all the components within the more porous light facies.

Results from a linear regression analysis provided an additional statistical support for the identification of the main components contributing to the variability of the sedimentary density in the core 33C. Only independent variables having a physical expression as the concentration of lithic minerals, carbonates, TOC, N and siliceous phytoplankton families (*Chaetoceros r.s.*, centric and pennate

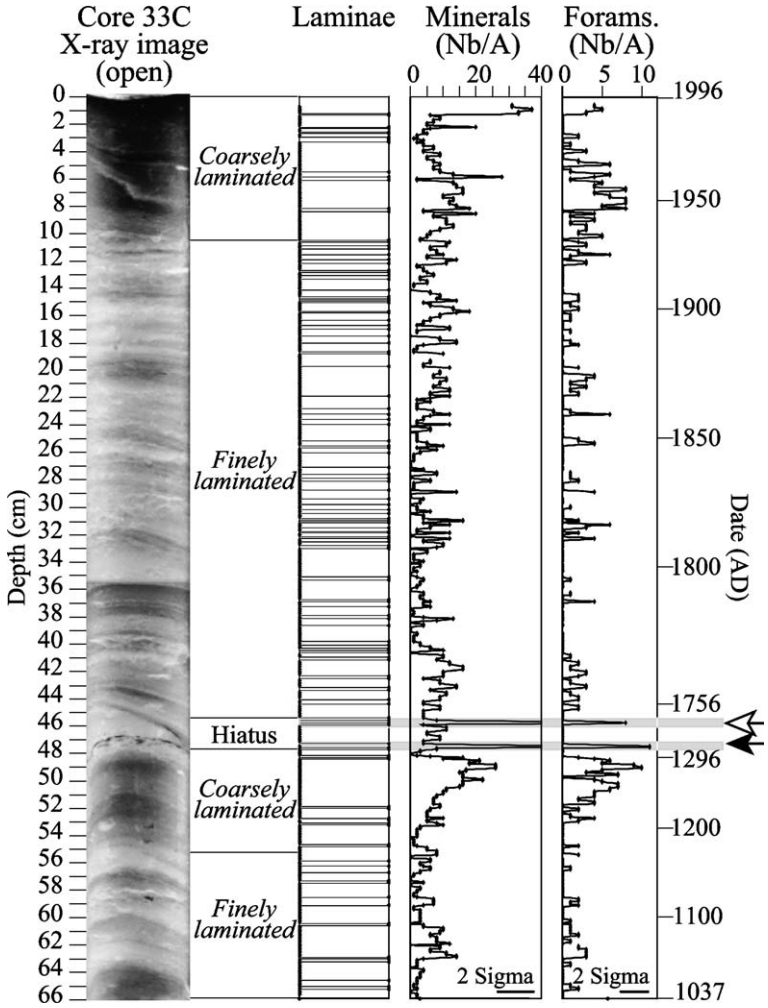

Fig. 9. High-resolution (every mm) variability of total minerals and foraminifera rests, with respect to the laminae and the occurrence of different styles of laminations in the core 33C. Calendars years are indicated on the right side. Black and white arrows indicate the location of two discontinuities associated with lenses anomalously enriched in lithic particles, incorporating an important hiatus in this sequence.

diatoms, silicoflagellates), expressed as absolute quantities, were included in this analysis. Considering the measured density as the dependent variable, the modelled density (adjusted density) includes the concentration of *Chaetoceros r.s.* as the most significant variable (p=0.00), followed by carbonates (p=0.05) and N (organic matter, p=0.10). Therefore, the standardized adjusted density can be successfully modelled through the equation:

$$\mathrm{Adj}D_x = 0.31 \times [\text{Chaetoceros r.s.}]_x + 0.33 \times [\text{Carbonates}]_x + 0.28 \times [\text{N}]_x,$$

where $\mathrm{Adj}D_x$ is the adjusted density value at the level x. The similarity between the measured and the adjusted density, characterized by a correlation coefficient of 0.74 (p<0.01), supports this result (Fig. 10).

A principal component (PC) analysis was carried out to relate variables contributing to the total variance of the sedimentary components in the core 33C. For this analysis, we considered only independent variables, excluding the GLMean, density and the concentration of opal. We included families of siliceous phytoplankton expressed as absolute quantities as well as the total number of

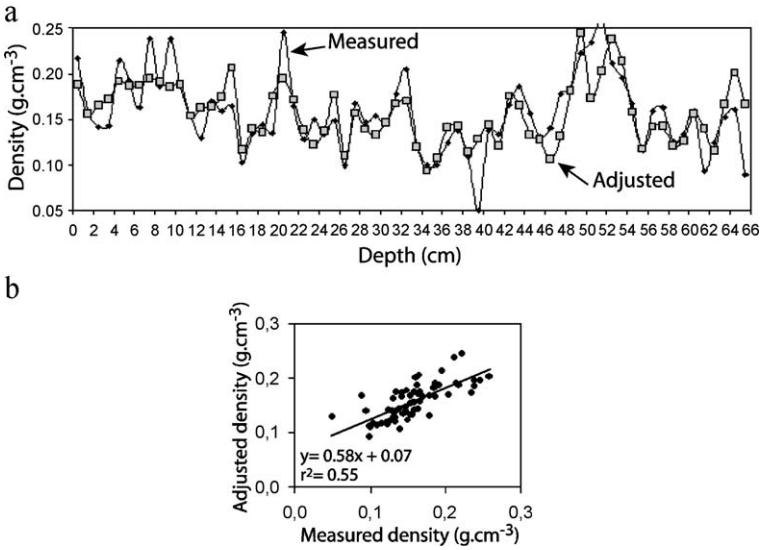

Fig. 10. (a) Comparison between the measured and the adjusted values of sedimentary density calculated from a linear regression modeling. The modeled adjusted density is a function of the number of valves per gram of *Chaetoceros r.s.*, the percentage of carbonates and the concentration of nitrogen. (b) Correlation between the measured and the adjusted density values shown in a. A significant correlation of r=0.74 (r^2=0.55) supports the accuracy of the model.

species, which provides some information about the diversity of the phytoplankton rests. The first three PCs explain 75% of the total variance (Fig. 11a). The PC_1 captures 40% of the variance, and is significantly correlated with components associated with upwelling-induced primary production indicators, as the concentration of lithic particles, *Chaetoceros r.s.*, TOC, N and carbonates (Fig. 11b). The PC_2, which captures 23% of the total variance, is well correlated with the absolute concentration of the centric and pennate diatoms and silicoflagellates, as well as with the total number of species, reflecting most probably changes in phytoplankton assemblages. Finally, the PC_3 captures 12% of the total variance and is significantly correlated with the HI (r=0.75, p<0.01) and inversely correlated with the C/N ratio (r=−0.82, p<0.01), reflecting most probably variations in the organic matter quality. These results support the hypothesis drawn from the observation of microfacies, suggesting that most of the textural and compositional variability observed in the sequences can be associated with variations in sedimentary fluxes driven by upwelling-induced primary production within the bay.

3.3. Sedimentary fluxes and paleoproduction inferences

Fluxes of TOC and carbonates were calculated for the core 32B and the top segment of the core 33C, showing a high variability (frequency and amplitude) during the last ~250 years (Fig. 12). This is particularly true in the case of the core 32B, which was subsampled according the limits of the laminations. Considering the improved chronology for both cores, the variability observed in both sequences (Fig. 12) reflects most probably ocean–climate variations at decadal and interdecadal time periods. Altogether, we observe an increase of these fluxes from the second half of the 19th century and increased values during the 20th century. This pattern is coherent with the flux of *Chaetoceros r.s.*, suggesting an intensification of the upwelling events and increased primary production rates during this last period.

Considering the variability of the first principal component as representative of components associated with upwelling-induced primary production, we can take the standardized anomaly of this PC (PC_1-Std) as an index of primary production within the bay. The evolution of this index shows a similar pattern

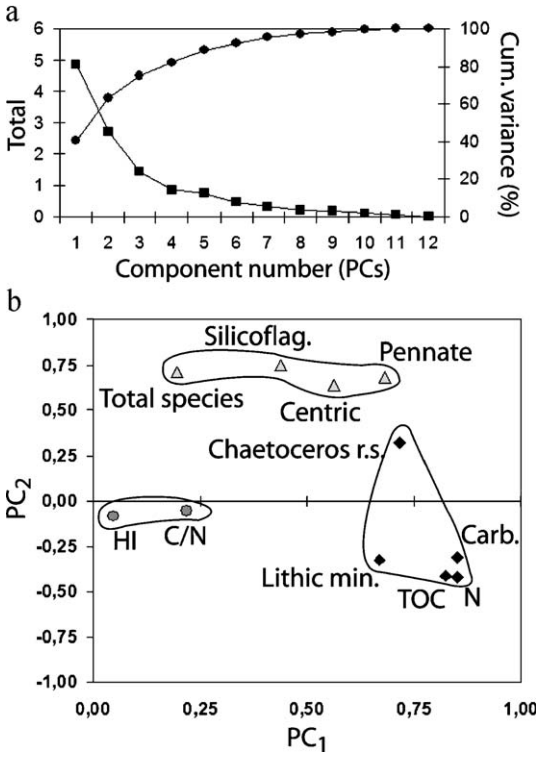

Fig. 11. (a) Eigenvalues and cumulative variance for the principal components associated to the variability of the sedimentary components in the core 33C. The first three PCs capture 75% of the total variance, giving a statistically valid representation of the total variance. (b) Correlation coefficients of the sedimentary components included in the principal component analysis with respect to the most significant two PCs.

with respect to those for the sedimentary fluxes, suggesting an increment of primary production from the second half of the 19th century, important variations at the end of this century and increased primary production during mostly the 20th century (Fig. 12).

4. Discussion

4.1. Sedimentation processes and ecological implications

The overall results are consistent with the dominancy of a relatively rhythmic hemipelagic sedimentation process, characterized by high fluxes of biogenic remains derived from primary production, in the central part of the basin. Beside the persistent bottom hypoxia inferred from the dominancy of *B. seminuda*, among the foraminifera rests, the preservation of agglomerated organic matter together with unfragmented phytoplankton remains and some monospecific levels of large centric diatoms must be associated with a rapid transit through a shallow water column (125 m maximum depth), which limits grazing-related processes. The high concentrations of *Chaetoceros r.s.* and the occurrence of agglomerates of these biogenic particles (Plate IC), together with the occurrence of agglomerated organic matter, suggest that this rapid settling should be enhanced by efficient mechanisms of flocculation immediately after the phytoplankton blooms (e.g. self-sedimentation; Grimm et al., 1997), induced by the exudation of carbohydrates from diatom cells, which favours the generation of transparent gels (Transparent Exopolymer Particles: TEP; Alldredge and Crocker, 1995). The observation of high concentrations of TEP in sediments from these laminated sequences supports the last hypothesis (Mari, personal communication, 2002). This type of transfer mechanism, together with the high rates of primary production estimated within the Mejillones bay (Marín et al., 2003), could explain the high concentration of TOC in these sediments, with respect to the general decreasing trend observed from the south to the north along the Chilean margin (Hebbeln et al., 2000). Considering the primary production value of 107 mg C cm^{-2} $year^{-1}$ estimated by Marín et al. (1993) for the period 1990–1991 within this bay, and taking into account the TOC flux of 1.2 mg C cm^{-2} $year^{-1}$, calculated from the first sample of the core 33C, representing the period 1989–1996, we suggest a preliminary estimation of the preserved production around 1.13% within this basin.

Through a regional study of surface sediments along the Chilean margin (between 22°S and 44°S, and from different water depths), supported by sediment trap surveys at 30°S (Romero et al., 2001), Romero and Hebbeln (2003) distinguished five marine diatoms assemblages: the coastal upwelling group, tropical/subtropical, southern cold waters, benthic and coastal planktonic, and one freshwater assemblage. Among the 61 species determined from sediment samples of the core 33C, those associated to the upwelling assemblage are: resting spores of *Chaetoceros coronatus*, *Chaetoceros debilis*, *Chaeto-*

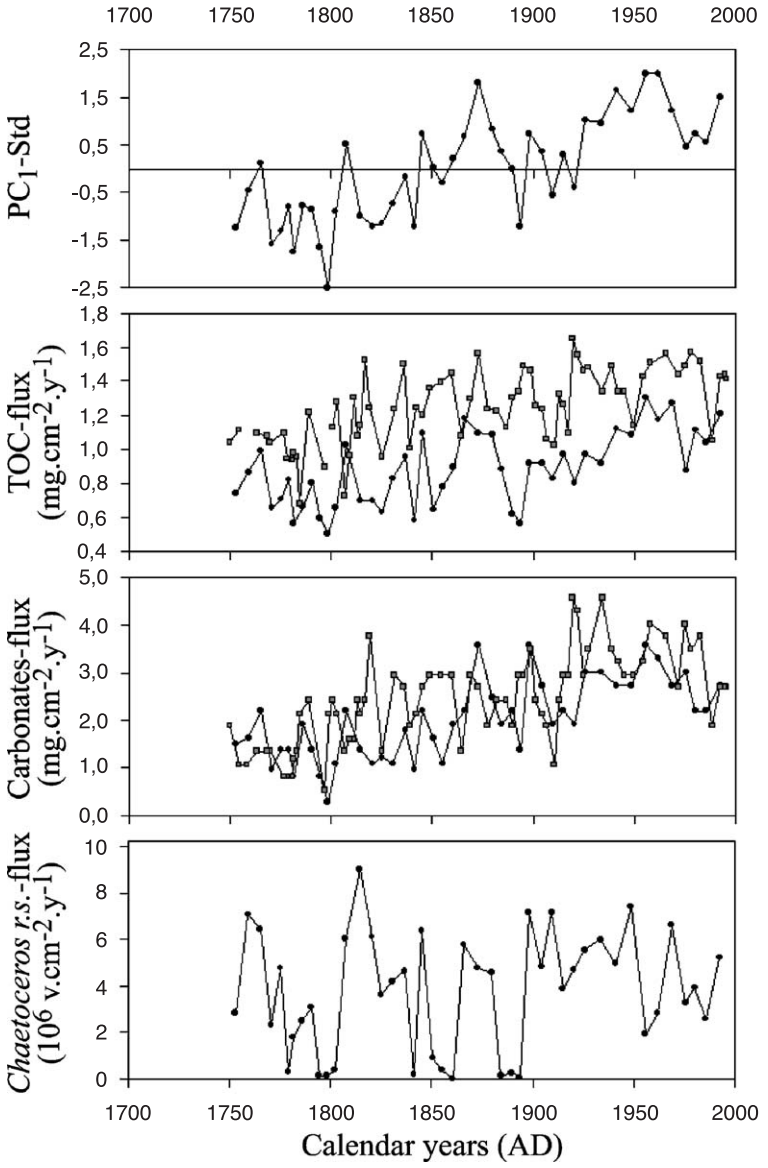

Fig. 12. Evolution of the sedimentary fluxes calculated for the cores 33C and 32B, and standardized anomaly of the PC_1, which is taken as a primary production index, during the last roughly ~250 years.

ceros didymus, *Chaetoceros holsaticus*, *Chaetoceros radicans*, *Chaetoceros subsecundus* and undetermined *Chaetoceros* sp., together with vegetative cells of *Skeletonema costatum* and *Thalassionema nitzschioides*. According to detailed oceanic surveys within the Mejillones bay, the association between *Chaetoceros r.s.* and *S. costatum* reflects a post-bloom assemblage related to a strong thermal stratification of the water column, while the association between *Chaetoceros r.s.* and *T. nitzschioides* reflects strong seasonal upwelling events (Rodríguez and Escribano, 1996; Rodríguez, personal communication, 2002). Among the tropical/subtropical assemblage of Romero and Hebbeln (2003), we recognized vegetative cells of the species *C. didymus*, *Planktoniella sol*, *Thalassiosira ferilineata*, *Thalassiosira lineate* and

Fragilariopsis doliolus. The coastal planktonic assemblage is represented by vegetative cells of *Actinocyclus curvatulus*, *Thalassiosira aestivalis*, *Thalassiosira eccentrica* and *Thalassiosira oestrupii* var. *venrickae*. Finally, among the benthic assemblage we recognized vegetative cells of the species *Cocconeis costata*, *Cocconeis dirupta*, *Cocconeis fasciolata*, *Cocconeis fluminensis*, *Cocconeis pediculus*, *Cocconeis scutellum*, *Delphineis surirella* and *Grammatophora marina*.

The contribution of the different phytoplankton assemblages to the variability of the total valves for the entire core 33C is shown in Fig. 13. The upwelling assemblage represents between 55% and 91% of the total phytoplankton valves, the concentration of *Chaetoceros r.s.* representing between 75% and 100% of this association. These observations confirm the relevancy of the upwelling system driving high sedimentary fluxes in this basin. The tropical/subtropical and coastal planktonic assemblages represent between % and 11%, and between 0 and 7%, respectively. The increase of the concentration of these assemblages in some levels where the upwelling association diminishes is coherent with the microscopic observations which suggest that the more porous light facies are associated to diminished concentration of *Chaetoceros r.s.* and relatively higher concentration of centric and pennate diatoms. Finally, the concentration of the benthic assemblage varies between 0 and 2%, showing a low variation and contribution to the variability of the total phytoplankton valves in this core.

4.2. Origin of the laminations

The overall results from qualitative and quantitative analyses performed at different sampled intervals show that the occurrence of laminations is associated with textural and compositional changes between adjacent laminae. Among these changes, the higher density and concentration of *Chaetoceros r.s.* and organic matter within the dark facies, with respect to the relatively higher porosity and concentration of centric and pennate diatoms within the light facies, seems to be the most important characteristic. Thus, we interpret that the origin of laminations is associated with changes in the intensity of the net sedimentary fluxes of biogenic remains and organic matter, as the response to variations of the upwelling-induced primary production within the Mejillones bay. The higher concentration and greater mean grain size of the lithic particles within the dark laminae with respect to the light facies provide an additional support for the intensification of the upwelling events,

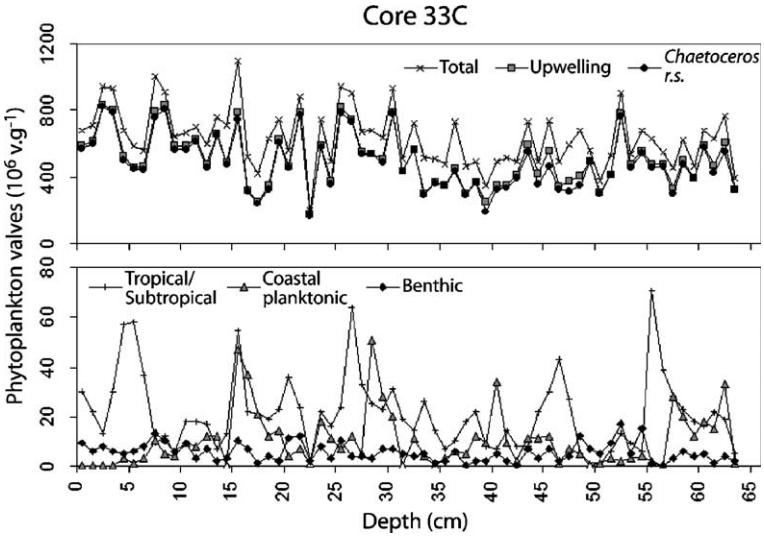

Fig. 13. Distribution of the phytoplankton assemblages, every cm, for the entire core 33C, following the association of species determined by Romero and Hebbeln (2003) for the Chilean margin.

through the intensification of the S–SW winds, during periods dominated by the deposition of dark facies.

This interpretation implies that intensified sedimentary fluxes of *Chaetoceros r.s.* and organic matter, possibly enhanced by efficient flocculation mechanisms, favour a more efficient burial of the organic carbon as well as of the labile components of the organic matter. From geochemical results regarding the concentration of trace metals from cores retrieved in this bay, Valdés and Ortlieb (2001) suggested that dominant darker intervals represent periods of intensified hypoxia in the bottom segment of the water column with respect to those characterized by a higher variability of laminations. Therefore we suggest that the high values of TOC together with the higher concentration of organic matter within the dominant dark facies could be explained by: (1) high primary production rates inducing important sedimentary fluxes; (2) increased hypoxia in the water column due to an increased consumption of oxygen: and (3) increased burial efficiency of the organic carbon and the organic matter, including the labile fraction. This hypothesis is consistent with the higher concentration of cadmium and organic matter in dominant dark segments of the core 32E, close from the core 32B, as shown by Valdés et al. (2003).

Altogether, we interpret that relatively lower sedimentary fluxes of *Chaetoceros r.s.* and organic matter reduce the burial efficiency and produce a sediment characterized by higher porosity, due to the relative rise of the concentration of other phytoplankton remains. The observations of microfacies and the variability of the phytoplankton assemblages shown in Fig. 13, particularly the high amount of tropical/subtropical and coastal planktonic diatoms in some levels, suggest that some light laminae (or part of them) were deposited during episodes of ENSO-like oceanographic conditions. Actually, the occurrence of some monospecific lenses of large diatoms as *C. gigas*, which represent short-lived events at the surface of the ocean, could be associated with the occurrence of variable and mixed water masses, possibly related with El Niño events (Rodríguez, personal communication, 2002). Scanning electron microscope observations and high-resolution qualitative and quantitative analyses of phytoplankton composition are needed to test this hypothesis.

Considering a sedimentation rate of 0.156 cm $year^{-1}$ calculated for the entire core 32B and the top segment of the core 33C (Vargas et al., in press), and taking into account the thickness variability, from 1 mm to several cm, of the laminae, we surmise that the laminations represent depositional periods ranging from seasons up to decades. Consequently, the occurrence of different lamination styles within the sequences can be related with different frequencies of ocean–climate variations inducing changes of the intensity of the upwelling events and primary production rates. A similar interpretation has been proposed to explain the occurrence of different thickness of laminae in the Santa Barbara basin (California), suggesting that the variation in thickness and assemblage of diatom ooze laminae is most probably related to the amount of the phytoplankton fluxes, controlled by upwelling-induced primary production (Bull and Kemp, 1996). On another hand, recent work (King et al., 1995) showed a reduction of the number of benthic foraminifera in well-preserved laminated diatomaceous oozes with respect to non-laminated sediments, suggesting some microscopic physical obliteration of the laminae due to benthic activity in the latter. Fig. 9 shows that the increase of the concentration of foraminifer remains, mainly *B. seminuda*, occurs in dominant dark, coarsely laminated segments of the cores 33C, with respect to the sections characterized by higher variability. However, the occurrence of thin laminae within these segments suggests that this effect should be less important with respect to the variations of the upwelling and primary production intensities, proposed just before. Moreover, and as revealed by microfacies and semi quantitative observations from samples of the core 33C, the higher relative concentration of the planktonic species *G. bulloides* together with *B. seminuda* in dark laminae and dominant dark sections is coherent with the previous interpretation of intensified hypoxia associated with strong influence of the upwelling events during the deposition of these facies. More precise quantitative studies regarding the comparison between the benthic and planktonic foraminifera could provide relevant information about the relationship between the intensity of the upwelling events and the bottom hypoxia in this basin.

4.3. Trends of upwelling and primary production variations

The sedimentation mechanisms proposed to explain the occurrence of laminations as well as the high variability of sedimentary fluxes is consistent with the conceptual model based on in situ measurements, proposed by Marín and Olivares (1999) and Marín et al. (2003) to explain seasonal increases of the primary production rates within the Mejillones bay. At seasonal scale, the intensification of the upwelling events and primary production within the bay are explained by the intensification of the alongshore S–SW winds, driven by strong land–sea thermal contrast during hours of highest insolation (Rutllant et al., 1998; Strub et al., 1998; Marín and Olivares, 1999). A similar climate mechanism can explain decadal to interdecadal increases of the sedimentary TOC flux (preserved production) observed in sediment cores. Rutllant et al. (1998) showed a net intensification (of about 1.5 m/s) in the strength of S–SW winds, since the end of 1976, as the result of a lower frequency of cloudiness during the hours of highest insolation, implying the intensification of the most relevant climate constraints for the primary production within the bay: the S–SW wind and the solar radiation (Marín and Olivares, 1999). On a Pacific Ocean basin scale, ENSO-like interdecadal variability has been documented for the second half of the 20th century, suggesting significant ocean–climate variations along the western margin of South America (Zhang et al., 1997, Mantua et al., 1997; Garreaud and Battisti, 1999). Besides, decadal ocean–climate variability has been reported from corals in the tropical Pacific Ocean (e.g. Linsley et al., 2000; Cole et al., 2000). We suggest that the high-frequency variations of the sedimentary fluxes observed in cores 33C and 32B (Fig. 12) reflect these types of basin scale ocean–climate variability in the Pacific Ocean. This interpretation also provides an additional explanation for the occurrence of different lamination styles within the sequences.

At secular time scale, the long-term intensification of the upwelling-induced primary production from the second half of the 19th century, inferred from the observation of the sedimentary fluxes in both cores, seems to be linked to a freshening and sea surface cooling inferred from coral data in the south western tropical Pacific Ocean (Hendy et al., 2002), suggesting major basin scale ocean–climate changes in this period. The increase of the total number of fish scales in the top segment of the core 33C (Fig. 4), corresponding mostly to *Engraulis ringens* (anchovy), also suggests major changes of ecological conditions in the south eastern Pacific Ocean. Altogether, interdecadal trends of fish scale abundance during the 20th century, as shown in Fig. 4, are similar to those described by Mantua et al. (1997) for the north Pacific Ocean. The Mejillones bay laminated sediments deserve further studies oriented toward the study of ecological changes associated with ocean–climate trends in the south eastern Pacific Ocean.

5. Conclusions

The composition of the laminated diatomaceous sediments of Mejillones bay is dominated by the high concentration of *Chaetoceros r.s.* and organic matter, which assess the strong control of upwelling events upon hemipelagic sedimentation processes. The thickness of the laminae ranges from 1 mm to several cm. Those laminae are associated with changes in density (porosity), due to the different concentration of phytoplankton rests, TOC and organic matter, carbonates and lithic particles. Dark laminae are generally characterized by higher concentration of *Chaetoceros r.s.*, TOC, organic matter, carbonates and lithic minerals with respect to the adjacent light laminae, which result from intensified net sedimentary fluxes due to strong upwelling events and high primary production rates. These last conditions induce intensified hypoxia within the bay and more efficient burial of the organic matter, favouring its preservation. Contrarily, light laminae are characterized by diminished concentration of *Chaetoceros r.s.* and the other components just mentioned, and relative increases of the concentration of centric and pennate diatoms, thus yielding a more porous sediment. These last conditions should be associated with relative diminished upwelling-induced primary production, as well as diminished hypoxia within the bay.

The presence of different lamination styles is interpreted as the result of different ocean–climate modes of variations, driving the intensity of the upwelling events and primary production rates. In

this sense, thicker dark laminae are associated with greater wind-driven upwelling intensity and primary production rates, relative to the adjacent light facies or sections showing higher variability. Ecological inferences from microfacies and phytoplankton assemblages suggest that some of the light laminae might be associated with major oceanographic events like ENSO. From the sedimentation rate estimates and the thickness variability of the laminations, it is inferred that one individual lamina represents periods of time ranging from seasons up to decades.

The variability of the sedimentary fluxes in both cores represents mostly ocean–climate variations at decadal interdecadal and secular time periods. Decadal and interdecadal variations of the upwelling and primary production should be associated with regional and Pacific Ocean basin scale climate trends. The intensification of the upwelling events and primary production since the second half of the 19th century and during the 20th century, as interpreted from both cores, appear to be contemporaneous to ocean–climate changes documented in the south western tropical Pacific Ocean (Hendy et al., 2002). This suggests a major basin scale climate change during this period.

Acknowledgements

This work was financed by the UR55; program PALEOTROPIQUE, Institut de Recherche pour le Développement (IRD). G. Vargas benefited from a scholar grant from IRD (DSF), while he completed his PhD in the Département de Géologie et Océanographie, Université de Bordeaux 1, Bordeaux (France). This is DGO-EPOC contribution number 1517.

The authors thank Nury Guzmán, Mónica Páez, Paola Irachet and Abdelffetah Sifeddine for their help with the preparation of samples, the foraminifer and fish scales analyses and obtention of geochemical data. Luis Rodriguez, José Rutllant and Jorge Valdés contributed to the discussion.

Dierk Hebbeln and Frank Lamy provided relevant suggestions for the first version of this paper.

During the editorial stage of this paper, two of our co-authors died quite prematurely. This paper is dedicated to both of them, Jean Jacques Pichon († 2003) and Jacques Bertaux († 2002).

References

Alldredge, A.L., Crocker, K.M., 1995. Why do sinking mucilage aggregates accumulate in the water column? Sci. Total Environ. 165, 15–22.

Bertaux, J., Fröhlich, F., Ildefonse, Ph., 1998. Multicomponent analysis of FTIR spectra: quantification of amorphous silica and crystallized mineral phases in synthetic and natural sediments. J. Sediment. Res. 68 (3), 440–447.

Bouma, A., 1964. Note on X-ray interpretation of marine sediments. Mar. Geol. 2, 278–309.

Brandhorst, W., 1971. Condiciones oceanográficas estivales frente a la costa de Chile. Rev. Biol. Mar. 14 (3), 45–84 (Valparaiso).

Bull, D., Kemp, A., 1996. Composition and origins of laminae in late Quaternary and Holocene sediments from the Santa Barbara Basin. In: Kemp, A.E.S. (Ed.), Palaeoclimatology and Palaeoceanography from Laminated Sediments. Geological Society London Special Publication 116, 143–156.

Calvert, S.E., Veevers, J.J., 1962. Minor structures of unconsolidated marine sediments revealed by X-radiography. Sedimentology 1, 296–301.

Cole, J., Dunbar, R., McClanahan, T., Muthiga, A., 2000. Tropical Pacific forcing of decadal SST variability in the western Indian Ocean over the past two centuries. Science 287, 617–619.

Escribano, R., 1998. Population dynamics of *Calanus chilensis* in the eastern boundary Humboldt current. Fish. Oceanogr. 7, 245–251.

Espitalié, J., Laporte, J.L., Madec, M., Marquis, F., Leplat, P., Paulet, J., Boutefeu, A., 1977. Méthode rapide de caractérisation des roches mères, de leur potential pétrolier et de leur degré d'évolution. Rev. Inst. Fr. Pét. 32, 23–42.

Ferraris, F., Di Biase, F., 1978. Hoja Antofagasta, Región de Antofagasta. Carta Geol. Chile vol. 30. Instituto de Investigaciones Geológicas, Chile. 48 pp., 1 map 1:250.000.

Garreaud, R., Battisti, D., 1999. Interannual (ENSO) and interdecadal (ENSO-like) variability in the Southern Hemisphere tropospheric circulation. J. Clim. 12, 2113–2123.

Gonzalez, H., Daneri, G., Figueroa, D., Iriarte, J.L., Lefevre, N., Pizarro, G., Quiñones, R., Sobarzo, M., Troncoso, A., 1998. Producción primaria y su destino en la trama trófica pelágica y océano profundo e intercambio océano–atmósfera de CO_2 en la zona norte de la Corriente de Humboldt (23°S): posibles efectos del evento El Niño 1997–98 en Chile. Rev. Chil. Hist. Nat. 71, 429–458.

Gonzalez, H., Ortiz, V., Sobarzo, M., 2000. The role of faecal material in the particulate organic carbon flux in the northern Humboldt Current, Chile (23°S), before and during the 1997-1998 El Niño. J. Plankton Res. 22 (3), 499–529.

Graham, W., Largier, J.L., 1997. Upwelling shadows as nearshore retention sites: the example of northern Monterey Bay. Cont. Shelf Res. 17, 509–532.

Grimm, K., Lange, C., Gill, A., 1997. Self-sedimentation of phytoplankton blooms in the geologic record. Sediment. Geol. 110, 151–161.

Hebbeln, D., Marchant, M., Freudenthal, T., Wefer, G., 2000. Surface distribution along the Chilean continental slope related to upwelling and productivity. Mar. Geol. 164, 119–137.

Hebbeln, D., Marchant, M., Wefer, G., 2002. Paleoproductivity in the southern Peru–Chile Current through the last 33,000 yr. Mar. Geol. 186, 487–504.

Hendy, E.J., Gagan, M.K., Alibert, C.A., McCulloch, M.T., Lough, J.M., Isdale, P.J., 2002. Abrupt decrease in tropical Pacific sea surface salinity at the end of Little Ice Age. Science 295, 1511–1514.

Hughen, K., Overpeck, J., Peterson, L., Anderson, R., 1996. The nature of varved sedimentation in the Cariaco basin, Venezuela, and its palaeoclimatic significance. In: Kemp, A.E.S. (Ed.), Palaeoclimatology and Palaeoceanography from Laminated Sediments. Geological Society London Special Publication 116, 171–183.

Iriarte, J.L., Pizarro, G., Troncoso, V.A., Sobarzo, M., 2000. Primary production and biomass of size-fractionated phytoplankton off Antofagasta, Chile (23–24°S) during pre-El Niño and El Niño 1997. J. Mar. Syst. 26, 37–51.

Kim, J.-H., Schneider, R., Hebbeln, D., Müller, P.J., Wefer, G., 2002. Last deglacial sea-surface temperature evolution in the Southeast Pacific compared to climate changes on the South American continent. Quat. Sci. Rev. 21, 2085–2097.

King, S.C., Kemp, A.E., Murray, J.W., 1995. Benthic foraminifer assemblages in Neogene laminated diatom ooze deposits in the eastern equatorial Pacific Ocean (Site 844). In: Mayer, L.A., Pisias, N.G., Janecek, T.R., Palmer-Julson, A., van Andel, T.H. (Eds.), Proc. Ocean Drill. Prog., Sci. Results vol. 138, 665–673.

Lamy, F., Hebbeln, D., Wefer, G., 1999. High-resolution marine record of climatic change in mid-latitude Chile during the last 28,000 years based on terrigenous sediments parameters. Quat. Res. 51, 83–93.

Lamy, F., Klump, J., Hebbeln, D., Wefer, G., 2000. Late Quaternary rapid climate change in northen Chile. Terra Nova 12, 8–13.

Laws, R.A., 1983. Preparing strewn slides for quantitative microscopical analysis: a test using calibrated microspheres. Micropaleontology 29, 60–65.

Lettau, H., Lettau, K., 1978. Exploring the World's driest climate. Report 101 IES, University of Wisconsin, Madison, USA.

Linsley, B., Wellington, G., Schrag, D., 2000. Decadal sea surface temperature variability in the subtropical South Pacific from 1726 to 1997 A.D. Science 290, 1145–1148.

Mantua, N.J., Hare, S.R., Zhang, Y., Wallace, J.M., Francis, R.C., 1997. A Pacific interdecadal climate oscillation with impacts on salmon production. Bull. Am. Meteorol. Soc. 78, 1069–1079.

Marchant, M., Hebbeln, D., Wefer, G., 1998. Seasonal flux patterns of planktic foraminifera in the Peru–Chile current. Deep-Sea Res., Part 1 45, 1161–1185.

Marchant, M., Hebbeln, D., Wefer, G., 1999. High resolution record of the last 13,300 years from the upwelling area off Chile. Mar. Geol. 161, 115–128.

Marín, V., Olivares, G., 1999. Estacionalidad de la productividad primaria en Bahía Mejillones del Sur (Chile): una aproximación proceso-funcional. Rev. Chil. Hist. Nat. 72, 629–641.

Marín, V., Rodríguez, L., Vallejos, L., Fuenteseca, J., Oyarce, E., 1993. Efectos de la surgencia costera sobre ela productividad primaria primaveral de Bahía Mejillones del Sur (Antofagasta, Chile). Rev. Chil. Hist. Nat. 66, 479–491.

Marín, V., Escribano, R., Delgado, L., Olivares, G., Hidalgo, P., 2001. Nearshore circulation in a coastal upwelling site off the Northern Humboldt current system. Cont. Shelf Res. 21, 1317–1329.

Marín, V., Delgado, L., Escribano, R., 2003. Upwelling shadows at Mejillones Bay (northern Chilean coast): a remote sensing in situ analysis. Invest. Mar. Valparaíso 31 (2), 47–55.

Meyers, P.A., 1994. Preservation of elemental and isotopic source identification of sedimentary organic matter. Chem. Geol. 144, 289–302.

Meyers, P.A., 1997. Organic geochemical proxies of paleoceanographic, paleolimnologic and paleoclimatic processes. Org. Geochem. 27 (5/6), 213–250.

Morales, C.E., Blanco, J.L., Braun, M., Reyes, H., Silva, N., 1996. Chlorophyll-*a* distribution and associated oceanographic conditions off northern Chile during the winter and spring 1993. Deep-Sea Res. 43, 267–389.

Navea, E., Miranda, O., 1980. Ciclo anual de las condiciones oceanográficas en Mejillones del Sur (Chile). Rev. Biol. Mar. (Valparaiso) 17, 97–133.

Ortlieb, L., Escribano, R., Follegati, R., Zuñiga, O., Kong, I., Rodríguez, L., Valdés, J., Guzmán, N., Iratchet, P., 2000. Recording ocean–climate changes during the last 2,000 years in a hypoxic marine environment off northern Chile (23°S). Rev. Chil. Hist. Nat. 73, 221–242.

Páez, M., Zúñiga, O., Valdés, J., Ortlieb, L., 2001. Foraminíferos bentónicos recientes en sedimentos micróxicos de la bahía Mejillones del Sur (23°S), Chile. Rev. Biol. Mar. Oceanogr. 36 (2), 129–139.

Rathburn, A.E., Pichon, J.-J., Ayress, M.A., De Deckker, P., 1997. Microfossil and stable-isotope evidence for changes in Late Holocene paleoproductivity and paleoceanographic conditions in the Prydz Bay region of Antarctica. Palaeogeogr. Palaeoclimatol. Palaeoecol. 131, 485–510.

Rodríguez, L., Escribano, R., 1996. Bahía Antofagasta y Bahía Mejillones del Sur: Observaciones de la temperatura, penetración de la luz, biomasa y composición fitoplanctónica. Est. Oceanol. 15, 75–85.

Rodríguez, L., Marín, V., Farías, M., Oyarce, E., 1991. Identification of an upwelling zone by remote sensing and in situ measurement, Mejillones del Sur Bay (Antofagasta-Chile). Sci. Mar. 55 (3), 467–473.

Romero, O., Hebbeln, D., 2003. Biogenic silica and diatom thanatocoenosis in surface sediments below the Peru–Chile Current: controlling mechanisms and relationship with productivity of surface waters. Mar. Micropaleontol. 48, 71–90.

Romero, O., Hebbeln, D., Wefer, G., 2001. Temporal and spatial variability in export production in the SE Pacific Ocean: evidence from siliceous plankton fluyes and surface sediment assemblages. Deep-Sea Res., Part 1 48, 2673–2697.

Rutllant, J., Fuenzalida, H., Torres, R., Figueroa, D., 1998. Interacción océano–atmósfera–tierra en la Región de Antofagasta (Chile, 23°S): Experimento DICLIMA. Rev. Chil. Hist. Nat. 71, 405–427.

Schrader, H.-J., Gersonde, R., 1978. Diatoms and silicoflagellates. In: Zachariasse, W.J., et al., (Eds.), Micropaleontological counting methods and techniques—an exercise on an eight

metres section of the lower Pliocene of Capo Rosello, Sicily, Utrecht Micropaleontol. Bull. 17, 129–176.
Schwerdtfeger, W., 1976. Climates of Central and South América. World Surv. Climatol., 12.
Staubwasser, M., Sirocko, F., 2001. On the formation of laminated sediments on the continental margin off Pakistan: the effects of sediment provenance and sediment redistribution. Mar. Geol. 172, 43–56.
Strub, T., Mesías, J., Montecino, V., Rutllant, J., Salinas, S., 1998. Coastal ocean circulation off western South America. In: Robinson, A.R., Brink, K.H. (Eds.), The Sea vol. 11. Wiley, New York, pp. 273–313.
Stuiver, M., Reimer, P.J., 1993. Extended ^{14}C database and revised CALIB radiocarbon calibration program. Radiocarbon 35, 215–230.
Takahasi, T., 1989. The carbon dioxide puzzle. Oceanus 32, 22–29.
Tissot, B.P., Welte, D.H., 1984. Petroleum Formation and Occurrence. Springer, Amsterdam, 699 pp.
Torres, R., Turner, D.R., Silva, N., Rutllant, J., 1999. High short-term variability of CO_2 fluxes during an upwelling event off the Chilean coast at 30°S. Deep-Sea Res. Part 1 46, 1161–1179.
Torres, R., Turner, D.R., Rutllant, J., Sobarzo, M., Antezana, T., Gonzalez, H., 2002. CO_2 outgassing off central Chile (31–30°S) and northern Chile (24–23°S) during austral summer 1997: the effect of wind intensity on the upwelling and ventilation of CO_2-rich waters. Deep-Sea Res. Part 1 49, 1413–1429.
Ulloa, O., Escribano, R., Hormazabal, S., Quiñones, R., González, R., Ramos, M., 2001. Evolution and biological effects of the 1997–98 El Niño in the upwelling ecosystem off northern Chile. Geophys. Res. Lett. 28 (8), 1591–1594.
Valdés, J., Ortlieb, L., 2001. Paleoxigenación subsuperficial de la columna de agua en la bahía Mejillones del Sur (23°S): Indicadores geoquímicos en testigos de sedimento marino. Invest. Mar. 29 (1), 25–35.
Valdés, J., López, L., Lo Mónaco, S., Ortlieb, L., 2000. Condiciones paleoambientales de sedimentación y preservación de la materia orgánica en bahía Mejillones del Sur (23°S), Chile. Rev. Biol. Mar. Oceanogr. 35 (2), 169–180.
Valdés, J., Ortlieb, L., Sifeddine, A., 2003. Variaciones del sistema de surgencia de Punta Angamos (23°S) y la Zona de Mínimo de Oxígeno durante el pasado reciente: una aproximación desde el registro sedimentario de la Bahía Mejillones del Sur. Rev. Chil. Hist. Nat. 76 (3), 347–362.
Vargas, G., 2002. Interactions océan-atmosphère au cours des derniers siècles sur la côte du Désert d'Atacama: analyse multi-proxies des sédiments laminés de la Baie de Mejillones (23°S). PhD Thesis, Université Bordeaux I, France, 290 pp.
Vargas, G., Ortlieb, L., Rutllant, J., 2000. Aluviones históricos en Antofagasta y su relación con eventos El Niño/Oscilación del Sur. Rev. Geol. Chile 27 (2), 155–174.
Vargas, G., Ortlieb, L., Chapron, E., Valdés, J., Marquardt, C., in press. Paleoseismic inferences from a high resolution marine sedimentary record in northern Chile (23°S). Tectonophysics (in press).
Zhang, Y., Wallace, J., Battisti, D.S., 1997. ENSO-like Interdecadal Variability: 1900–93. J. Clim. 10, 1004–1020.